


Superexchange coupling of donor qubits in silicon

Mushita M. Munia^{1,2,*} Serajum Monir^{1,2} Edyta N. Osika^{1,2} Michelle Y. Simmons^{1,2}
and Rajib Rahman^{1,2,†}

¹*School of Physics, University of New South Wales, Sydney, New South Wales 2052, Australia*

²*Silicon Quantum Computing Pty Ltd., Level 2, Newton Building, University of New South Wales, Kensington, New South Wales 2052, Australia*

 (Received 11 September 2023; accepted 28 November 2023; published 22 January 2024)

Atomic engineering in a solid-state material has the potential to functionalize the host with novel phenomena. STM-based lithographic techniques have enabled the placement of individual phosphorus atoms at selective lattice sites of silicon with atomic precision. Here we show that by placing four phosphorus donors spaced 10–15 nm apart from their neighbors in a linear chain, one can realize coherent spin coupling between the end dopants of the chain, analogous to the superexchange interaction in magnetic materials. Since phosphorus atoms are a promising building block of a silicon quantum computer, this enables spin coupling between their bound electrons beyond nearest neighbors, allowing the qubits to be separated by 30–45 nm. The added flexibility in architecture brought about by this long-range coupling not only reduces gate densities but can also reduce correlated noise between qubits from local noise sources that are detrimental to error-correction codes. We base our calculations on a full-configuration-interaction technique in the atomistic tight-binding basis, solving the four-electron problem exactly, over a domain of a million silicon atoms. Our calculations show that superexchange can be tuned electrically through gate voltages where it is less sensitive to charge noise and donor-placement errors.

DOI: [10.1103/PhysRevApplied.21.014038](https://doi.org/10.1103/PhysRevApplied.21.014038)

I. INTRODUCTION

Donor qubits in silicon are promising candidates for encoding quantum information in the solid state due to their long coherence times [1–3] and their technological link to the silicon platform of the electronics industry. Experimental advancements in the past decades have enabled the precision placement of phosphorus donors in silicon [4–8]. The platform of phosphorus donor-based quantum computing has been bolstered by key milestone achievements over the last decade, including single-shot spin readout [9], the realization of single-electron-spin and single-nuclear-spin qubits [10,11], and, more recently, two-qubit SWAP gates [12] and a three-qubit-donor quantum processor with universal logic operation [13]. Exchange coupling between the electronic spins of donors remains a key mechanism for fast coupling of two qubits [12,14]. The exchange interaction depends

on the overlap between the electronic wave functions and ultimately limits the separation of donor qubits to about 10–15 nm in silicon devices. Long-range coupling schemes through resonators and cavities have recently been explored in donor qubits [15–17]; however, these typically require additional fabrication and integration steps, adding complexity to the overall manufacturing process. Spacing out the qubits is beneficial from an architectural point of view in fault-tolerant quantum computing [18] as correlations between the qubits due to local noise sources can be minimized. An increase in separation also relaxes stringent gate-density requirements and offers more-independent electrostatic control of the qubits by reducing their capacitive crosstalk. For STM-patterned donors with phosphorus-doped in-plane gates, the density is already low [19], so this technique is particularly appealing.

In this work, we study long-range exchange coupling between the end spins of four single-donor (1P) quantum dots in a linear chain. With each donor containing a single electron, a superexchange coupling is found to emerge between the donors at the end of the chain. This third-nearest-neighbor interaction enables the qubits to be separated by 30–45 nm. Using atomistic full-configuration-interaction (FCI) calculations, we study the eigenvalues and eigenvectors of four electron spins across

*m.munia@unsw.edu.au

†rajib.rahman@unsw.edu.au

Published by the American Physical Society under the terms of the [Creative Commons Attribution 4.0 International](https://creativecommons.org/licenses/by/4.0/) license. Further distribution of this work must maintain attribution to the author(s) and the published article's title, journal citation, and DOI.

four 1P atoms in silicon. We investigate the regime of superexchange where the distant qubits can be coherently manipulated and provide guidelines on the appropriate donor placement to achieve this. We also investigate the role of the conduction-band valleys in superexchange for donor separation along different crystallographic directions. We simulate the system using realistic electrostatic potentials produced by the surrounding in-plane STM-patterned gates, where we demonstrate tunability of superexchange with gate voltages, a crucial requirement for the realization of electrically controlled singlet-triplet oscillations. Finally, we comment on the sensitivity of superexchange to charge noise and donor-placement errors, as well as the role of nuclear spins in singlet-triplet oscillations induced by superexchange.

Recent experiments and theoretical calculations have shown indirect coupling of distant electrons in quantum dots via a central empty mediator [20–24], a multielectron quantum dot [21,24–29] and a linear chain of singly occupied quantum dots [20,30,31]. However, to date, comprehensive studies have not been performed on long-range indirect coupling for donor qubits in silicon. Compared with electrostatically defined quantum dots, donor quantum dots in silicon typically have atomic-scale properties with wave-function length scales an order of magnitude less and a large quantity of orbital-valley energy splittings [32]. A single phosphorus donor can bind at most two electrons, with the nucleus having a net $1/2$ spin. Early papers on single donor qubits showed how the exact position and axis of separation of donor qubits can significantly affect their direct exchange, including effects such as exchange oscillations due to valley interference [33,34]. More-recent work has shown that these effects can be mitigated by separating the donors along specific crystallographic directions, by using multidonor quantum dots [35] or by applying strain or placing the donors close to the surface [33]. Highly tunable nearest-neighbor exchange has also been predicted [35] and demonstrated [12] in asymmetric donor quantum dots, showing that multielectron molecular physics can be tuned by gate voltages. However, the atomistic character of these donors and donor-quantum-dot systems needs to be accounted for when one is considering indirect couplings such as superexchange since the phenomenon emerges from individual nearest-neighbor exchange couplings.

II. METHODS

The exact calculation of a multielectron system is challenging because of the complicated and numerically intensive electron-electron interaction term in the Schrödinger equation [36]. The accuracy relies both on the quality of the basis states and the multielectron approximation. In semiconductor materials such as GaAs, eigenstates from effective Hubbard Hamiltonian [20,25,37] or simple

Fock-Darwin states are often used as basis states [21]. These are, however, unsuitable for silicon due to the multivalley states. The effective-mass approximation has also been used to calculate single-electron basis states for donors in silicon [38,39]. However, the theory does not provide a complete description of the band structure and can be inaccurate at higher energy levels. In contrast, the full-band atomistic tight-binding model has the potential to capture all intricate nuances of the wave function of phosphorus donors in silicon, hence its use in this work.

The commonest approximation for multielectron calculations is the Hartree-Fock method, which ignores the electron-electron correlations to minimize the complexity of the calculations. Use of configuration interaction, on the other hand, increases the accuracy in the treatment of many-body interactions but can be computationally intensive. This is particularly true for a multivalley material such as silicon, where only a few electron calculations are present in the literature [33,40]. In this work, we performed a state-of-the-art investigation combining atomistic basis states with a full-configuration-interaction method to calculate the energy levels of a four-electron donor system without compromising accuracy.

A. Atomistic full configuration interaction

The FCI method obtains the exact numerical solution of a many-body Schrödinger equation, limited by the number and quality of single-electron basis states. The single-electron basis states used here are calculated with use of a ten-band $sp^3d^5s^*$ atomistic tight-binding method in NEMO3D [41,42]. This approach uses a localized atomic orbital-based method with nearest-neighbor interactions. The tight-binding parameters are optimized to reproduce the bulk-silicon band structure [43]. The phosphorus donors are represented by a Coulomb potential with a central-cell correction at the donor site, which can successfully determine the experimentally measured energy spectra of donors in silicon [44,45].

A schematic representation of the simulations is illustrated in Fig. 1(a). There are four phosphorus donors placed in a chain, each with an electron. The end electron spins, Q_1 and Q_2 , are the qubits separated by R . The middle spins, M_1 and M_2 , work as mediators, with corresponding donors being separated by r_M . The separation between Q_1 and M_1 is r_1 and the separation between M_2 and Q_2 is r_2 . The simulation domains used in the calculations entail approximately 1.14 million atoms, which account for approximately 60 nm of silicon in the direction of separation and approximately 20 nm in the other two directions. The single-electron basis states, solved from a parallel Block Lanczos eigensolver, are used to calculate the antisymmetric Slater determinants of the multielectron problem. The lowest-two single-electron valley-orbital states

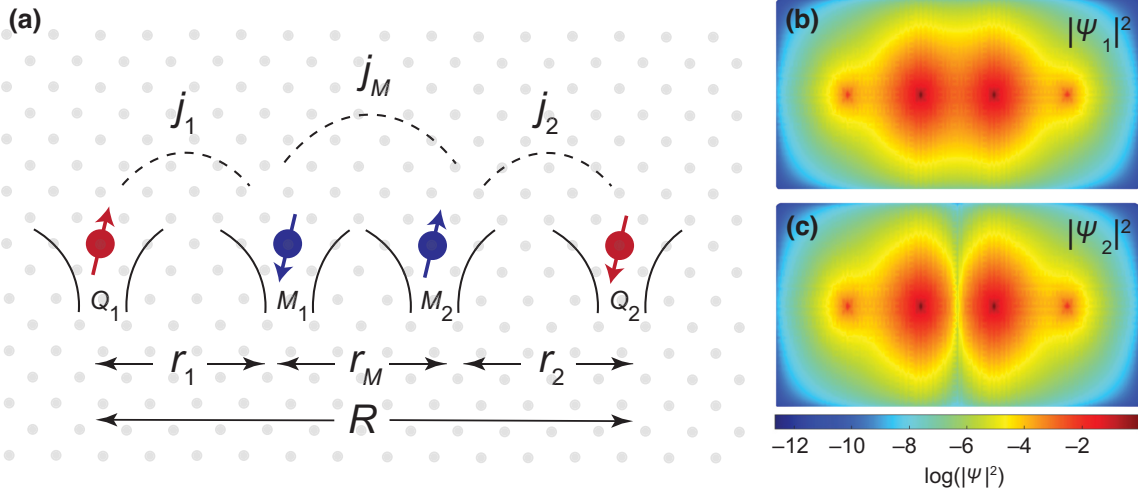


FIG. 1. Schematic representation of a simulation using four single phosphorus donors each with an electron. (a) Four phosphorus donors placed in the silicon crystal (gray), where the electrons localized in the two middle donors (blue) are mediators (M_1 and M_2) for the electron spins localized in the end donors (Q_1 and Q_2) (red). The separation of the blue mediator spins is r_M and their exchange coupling is j_M . The first qubit Q_1 is separated from the first mediator M_1 by r_1 (approximately 10 nm) and the second qubit Q_2 is separated from the second mediator M_2 by r_2 (approximately 10 nm). The corresponding exchange coupling between them is j_1 and j_2 , respectively. The total separation of qubits Q_1 and Q_2 is R (approximately 30 nm). The probability density of the lowest single-electron valley-orbital (b) bonding and (c) antibonding state on a logarithmic scale calculated with an atomistic tight-binding method.

of the system are shown in Figs. 1(b) and 1(c). Here we see bonding-state and antibonding-state formation in the middle-two donors M_1 and M_2 of a four-donor chain. The rest of the single-electron molecular basis states are shown in Fig. 2 in Supplemental Material [46], where we see the next-two valley-orbital states are localized mainly in the outer donor quantum dots.

The four-electron wave function is a superposition of various symmetry-permitted configurations of the Slater determinants. All possible integrals between the Slater determinants with pairwise electronic interaction operators are computed to capture Coulomb, exchange, and higher-order correlations. The four-electron Hamiltonian constructed from the Slater determinants is solved with use of the block Krylov-Schur algorithm within the Trilinos framework [47]. The number of single-electron basis states in FCI calculations is increased until the eigenvalues of the four-electron system converge within a chosen tolerance [46]. On average, 56 single-electron basis states are sufficient to reach convergence. The eigenvalue of the ground state is separated from the triply degenerate excited states by the indirect exchange coupling. We place the donor atoms at different separations and orientations in our simulations and calculate this exchange coupling.

B. Effective spin Hamiltonian

To analyze and interpret our FCI results, we compare them with an effective Hamiltonian model [30]. We can represent the four-spin system with a spin Hamiltonian

such as

$$H_{\text{eff}} = \frac{j_1}{4}\sigma_1\sigma_2 + \frac{j_M}{4}\sigma_2\sigma_3 + \frac{j_2}{4}\sigma_3\sigma_4, \quad (1)$$

where σ_i is a Pauli matrix corresponding to an electron spin located on the i th donor in the chain, j_M is the exchange coupling between the middle-two spins, M_1 and M_2 , j_1 is the exchange coupling between Q_1 and M_1 , and j_2 is the exchange coupling between Q_2 and M_2 ; see Fig. 1(a) for a schematic of the system.

We consider only the subspace with spin-zero states ($S_z = 0$) to construct the Hamiltonian as we are interested in the singlet-triplet oscillations in qubits Q_1 and Q_2 . When $j_1, j_2 \ll j_M$, we can isolate the low-energy states of the four-electron spin Hamiltonian using a Schrieffer-Wolff transformation. In that case, the effective Hamiltonian in a Heisenberg-exchange form, H_{SW} [30] becomes

$$H_{\text{SW}} = \frac{J_{\text{SW}}}{4}\sigma_1\sigma_4, \quad (2)$$

$$J_{\text{SW}} = \frac{j_1 j_2}{2j_M} \left[1 + \frac{3(j_1 + j_2)}{4j_M} \right],$$

In the regime where $j_1, j_2 \ll j_M$, the lowest-energy eigenstates are characterized by the singlet state formed within the two middle quantum dots and singlet or triplet states formed within the outer quantum dots [30]. The energy difference, ΔE , between the lowest long-distance

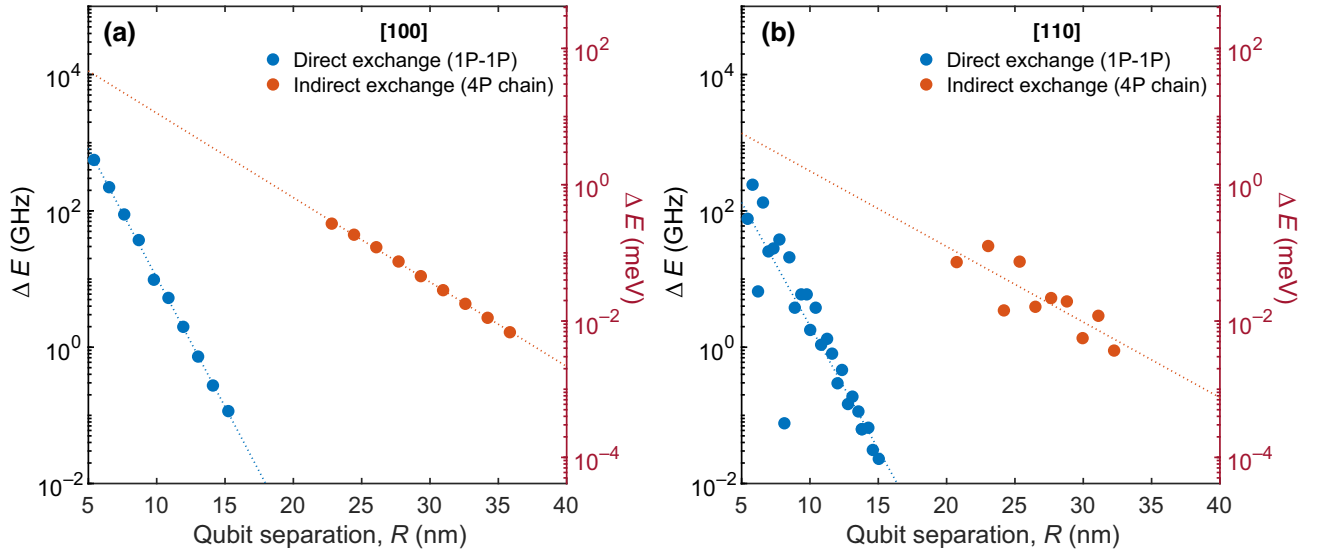


FIG. 2. Comparison of indirect and direct exchange coupling of 1P donors in silicon calculated with use of atomistic FCI. (a) Comparison of indirect exchange (4P chain) of the end spins (red dots) with nearest-neighbor exchange coupling (1P-1P) (blue dots, replicated from Ref. [35]) along the [100] direction. Dashed lines provide linear fits to both datasets. Here we see that the indirect exchange is greater than the nearest-neighbor exchange, with the exponential dependence on separation being less steep for indirect coupling. (b) Same as (a) but along the [110] direction. Here we see a similar trend in terms of the comparison between direct and indirect exchange as for the [100] direction. However, we also observe oscillations in the exchange coupling along this crystalline orientation due to valley quantum interference.

singlet and triplet states, i.e.,

$$\begin{aligned} S^I &\approx 1/\sqrt{2}(|\uparrow S \downarrow\rangle - |\downarrow S \uparrow\rangle) \\ T_0^I &\approx 1/\sqrt{2}(|\uparrow S \downarrow\rangle + |\downarrow S \uparrow\rangle) \end{aligned} \quad (3)$$

is what we call “superexchange” (ΔE) in this paper; see Fig. 3(a) for the energy-level diagram of the system. For $j_1, j_2 \ll j_M$, the middle-quantum-dot singlet manifold is well separated from all the middle-quantum-dot triplet states desirable for coherent coupling of the outer spins only, without any interference from the middle-quantum-dot spins.

III. RESULTS AND DISCUSSION

A. Equal nearest-neighbor separation of donors

We first analyze the equidistant case, where the separation between each neighboring pair of donors is equal, $r_1 = r_2 = r_M = R/3$; see Fig. 1. Here we have approximately equal values of exchange coupling between each pair of donors, i.e., $j_1 \approx j_2 \approx j_M$. In Fig. 2 (with red dots), we show the values of the indirect exchange coupling for these equispaced donors (4P chain) with constant but increasing separation between the dots along the [100] (left) and [110] (right) directions in the silicon crystal, calculated with use of FCI. For comparison, we also plot (with blue dots) the direct-exchange values for two donors, i.e., 1P-1P system, separated by R , as previously calculated in

Ref. [35]. Looking at the fitted dashed lines between the 4P chain and 1P-1P cases, we can see that the presence of the mediator donors dramatically increases the exchange coupling between the two outer spins. The indirect exchange coupling for a donor chain with R of about 25 nm reaches approximately 10^2 GHz (approximately 10^{-1} meV), while direct exchange coupling for the same separation without the presence of mediators would fall below 10^{-4} GHz (10^{-7} meV) (extrapolated from the dataset in Ref. [35]).

We also see that the direct exchange decays much faster than the indirect exchange by comparing the slope of the two plots, which is true for both the [100] crystal direction and the [110] crystal direction. For the [100] case in Fig. 2(a), the slope of the fitted dashed line for the direct exchange as a function of qubit separation is approximately $-0.38/\text{nm}$, whereas the slope for the indirect exchange is approximately $-0.12/\text{nm}$. Similarly in the [110] case in Fig. 2(b), the slope of the fitted line for the direct exchange is approximately $-0.36/\text{nm}$, whereas the slope for the indirect exchange is approximately $-0.11/\text{nm}$. In general, the indirect exchange decays almost 3 times less with donor separation than the direct exchange. This dependency on distance lets the qubits be well separated in the device and allows less-correlated noise between them while maintaining strong spin coupling. Since the nearest-neighbor exchange coupling has an exponential dependence with increasing separation of the donors, one might expect superexchange to change as an exponential function of $r_1 + r_2 - r_M$; see

Eq. (2). On the contrary, the nearest-neighbor exchange coupling changes as an exponential function of the qubit separation $R = r_1 + r_2 + r_M$, which results in a faster decay of direct exchange than indirect exchange.

We observe no oscillations in the exchange coupling when the donors are separated in the [100] direction, whereas we see oscillations in the exchange energy for separation in the [110] direction, a signature of intervalley quantum interference arising from the band structure of silicon [33,35,48].

B. Different regimes of superexchange from the effective spin Hamiltonian

To obtain superexchange and coherent control between the electron spin qubits at the end of chains Q_1 and Q_2 ,

it is essential that the middle spins M_1 and M_2 form a singletlike state. Otherwise there will be additional oscillations originating from the middle spins impeding coherent manipulation of the qubits. Thus we are looking for an operational regime where the ground state and the first excited state are well separated from the higher-energy states in which the indirect coupling can be termed “superexchange.” In Fig. 3(a) we plot the energies of all the eigenstates of the effective Hamiltonian H_{eff} as a function of $j_{1,2}/j_M$ varying from 0 to 1. When the outer spins are weakly coupled with the middle spins ($j_{1,2}/j_M \approx 0$), we see two clear branches of energy states separated by d , but the separation between the branches decreases as $j_{1,2}/j_M \approx 1$.

In Fig. 3(b), we plot the energy difference between the two-lowest states as a function of $j_{1,2}/j_M$ as calculated

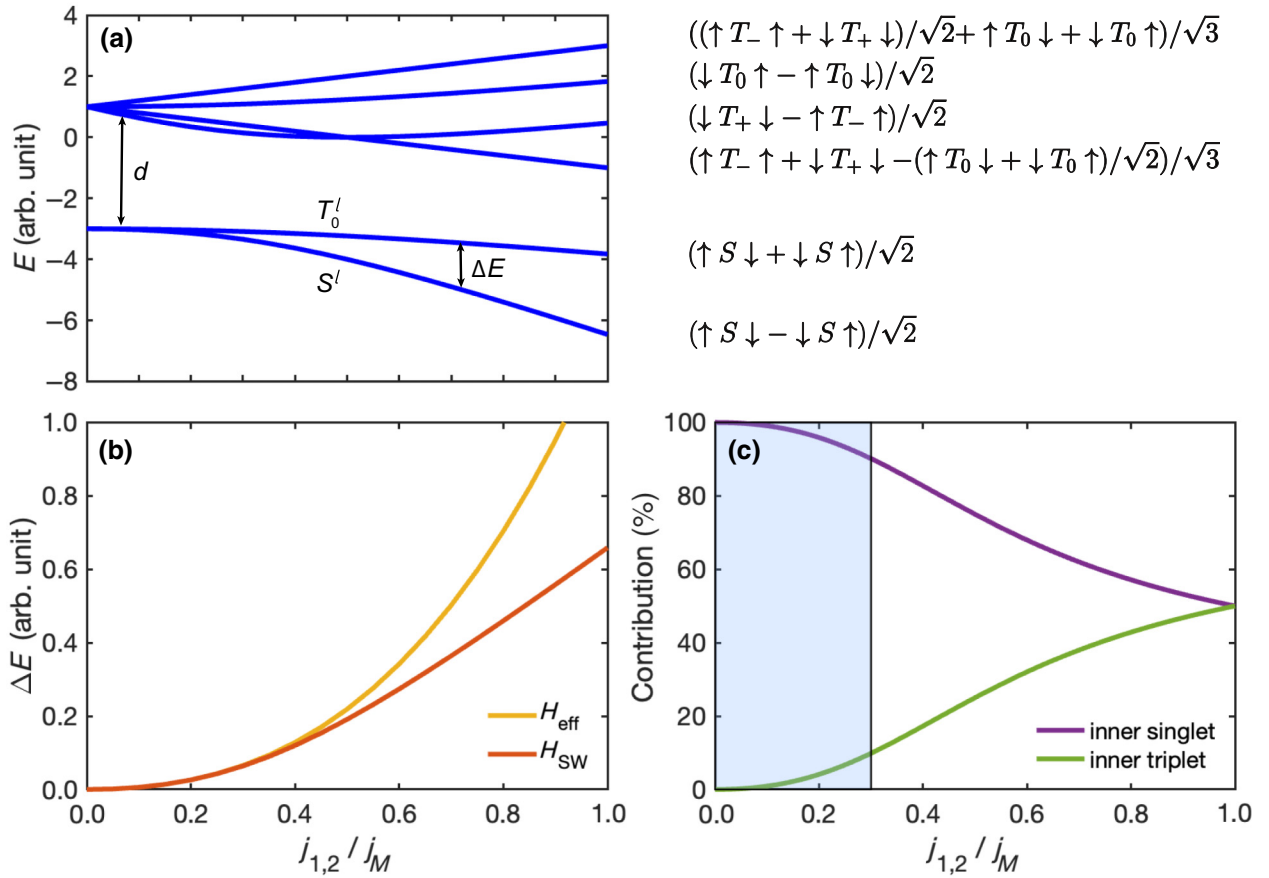


FIG. 3. Estimate of exchange-coupling strength from the spin Hamiltonian. (a) Energies of four-electron eigenstates calculated with the effective Hamiltonian H_{eff} as a function of $j_{1,2}/j_M$. The two-lowest states (spanned by $|\uparrow S \downarrow\rangle$ and $|\downarrow S \uparrow\rangle$) are well separated from the higher states when $j_{1,2}/j_M$ is smaller. The separation of these two energy levels is the superexchange ΔE . The labels on the right refer to the dominant contribution of the corresponding energy states when $j_{1,2}/j_M \approx 0$. (b) Comparison of the exchange coupling, ΔE , calculated from the effective spin Hamiltonian and the Schrieffer-Wolff Hamiltonian shows that for $j_{1,2}/j_M$ up to approximately 0.3, the superexchange from H_{eff} and H_{SW} is the same since the Schrieffer-Wolff Hamiltonian is a valid approximation of the spin Hamiltonian. Beyond this regime, their behavior diverges significantly because the Schrieffer-Wolff transformation no longer holds, indicating the development of an admixture in the singletlike state of the middle-two spins. (c) Contribution of the inner-singlet and inner-triplet basis states to the ground state of H_{eff} as a function of $j_{1,2}/j_M$. Here we see that as $j_{1,2}/j_M$ increases, the singlet contribution from the inner mediator spins decreases, and the triplet contribution increases. At $j_{1,2}/j_M = 1$, the ground state has equal contributions from singlet and triplet mediator spin states. The contribution of the inner singlet to the ground state is more than 90% for $j_{1,2}/j_M < 0.3$ (shaded region).

from H_{eff} and H_{SW} . These two-lowest states are the long-distance singlet and triplet states, namely, S^l and T_0^l . Here we see that, in the regime where $j_{1,2}/j_M \approx 0$, the solutions from the effective spin Hamiltonian and the Schrieffer-Wolff Hamiltonian are the same since the assumption of the transformation is valid here. As $j_{1,2}/j_M$ increases, the two solutions start to diverge, suggesting the Schrieffer-Wolff transformation no longer holds. The two-lowest energy states (spanned by $|\uparrow S \downarrow\rangle$ and $|\downarrow S \uparrow\rangle$) are no longer well separated from the excited states and there are now tripletlike admixtures in the singletlike state of the middle-two spins.

In Fig. 3(c), we can see the contributions in the ground state S^l of the inner-quantum-dot singlet states (i.e., $|\uparrow S \downarrow\rangle$ and $|\downarrow S \uparrow\rangle$) and inner-quantum-dot triplet states (all the remaining basis states). When $j_{1,2}/j_M = 1$ (i.e., the equidistant case where all donors are equally separated), the inner-quantum-dot singlet and triplet contributions in S^l are both approximately 50% and we no longer have a well-defined two-level system of S^l and T_0^l , but we now have contributions from the four higher states shown in Fig. 3(a). As $j_{1,2}/j_M$ decreases, the contribution of the inner-quantum-dot singlet reaches more than 90%, where $j_{1,2} \lesssim 0.3j_M$ (shaded region). This regime can be considered as a threshold for coherent operation of the qubits. However, we note that the threshold we mention

here ($j_{1,2}/j_M \approx 0.3$) is not the upper limit of the coherent regime. The ratio should ideally be very close to 0.

C. Modulating superexchange by changing the middle-donor separation

To explore the coherent-control regime of the four-donor chain using our FCI calculations, we switch from the equidistant case discussed in Fig. 2 to a chain with varied $r_{1,2}/r_M$ ratios; see Fig. 4. Here we present values of the indirect exchange coupling for chains oriented along the [100] and [110] directions in Figs. 4(a) and 4(b), respectively, as a function of middle-donor separation while we keep the outer-donor separation R constant. The lower-middle-donor separation corresponds to a higher exchange coupling j_M and lower j_1 and j_2 couplings, moving the system closer to the regime well described by the Schrieffer-Wolff approximation. In general, we see from Fig. 4 that the exchange coupling exponentially decreases as we decrease the middle-donor separation. The dashed gray line represents the separation where $r_1 = r_2 = r_M$. The exchange coupling shows two different dependencies on either side of this point. The first is where the distance between the middle donors is smaller than r_1 or r_2 and the second is where it is large. For donors separated along

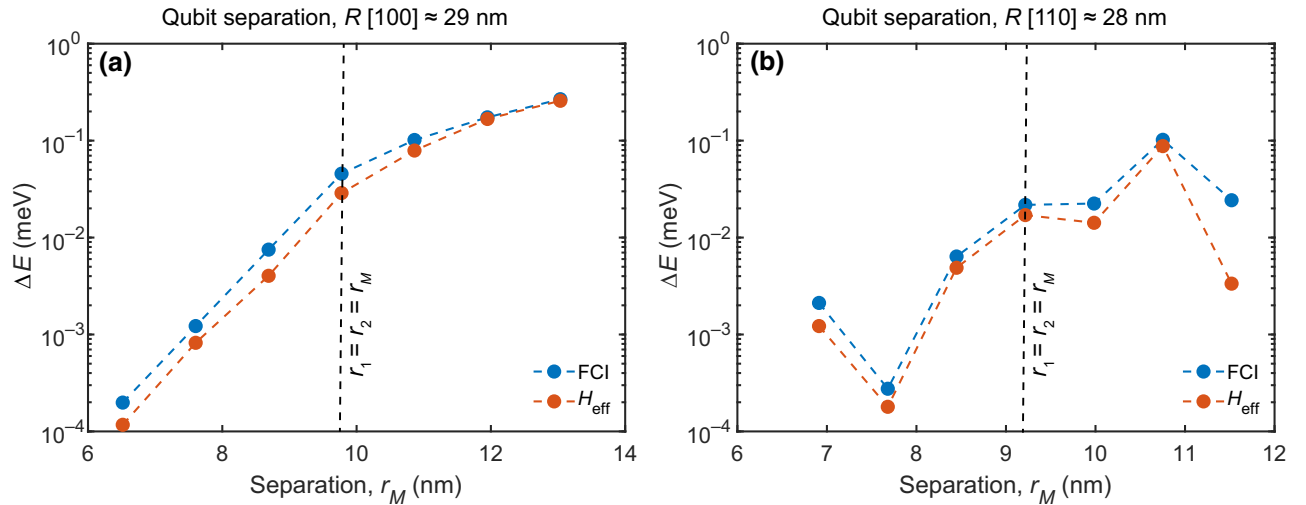


FIG. 4. Exchange coupling as a function of different middle-donor separations, r_M . The exchange coupling ΔE is calculated with use of atomistic FCI for different separations of the middle donors r_M in (a) the [100] direction and (b) the [110] direction while the total outer-qubit separation is kept fixed ($R = 29.3274$ nm for the [100] direction and $R = 27.648$ nm for the [110] direction). The system is symmetric ($r_1 = r_2$) to the end donors. The results show that the dependence of exchange energy changes on either side of the equidistant separation (dashed gray line) for all donors. The dashed line indicates where $r_1 = r_2 = r_M$, and the left region of this line, where $r_1 = r_2 > r_M$, is where the two middle donors form a singlet state and the exchange coupling between the end donors is termed “superexchange.” We compare our FCI results with the effective spin Hamiltonian, H_{eff} of Eq. (1) with $j_{1,2}$ and j_M extracted from Ref. [35]. For both cases, the results show reasonable agreement with each other. We attribute any differences mainly to the fact that the total confinement potential of four donors is deeper than that of two donors, which results in a slightly greater exchange coupling ΔE in our atomistic FCI calculations.

the [110] direction, we see clear oscillations in ΔE as a function of r_M .

As we discussed in the previous section, the equidistant-donor chain is not suitable for coherent manipulation of distant spins due to the admixture of states. The right side of the dashed gray line, where $r_1 = r_2 \leq r_M$, is therefore not valid for operating qubits. To specify the limits of these different regimes, we use the values of direct exchange from the 1P-1P results in Ref. [35] to find $r_{1,2}$ and r_M and the corresponding threshold. Decreasing the separation of the middle quantum dots gives rise to a value of the superexchange that decreases exponentially, while increasing the inner-singlet contributions to the ground state; see Table 1 in Supplemental Material [46]. So there is a trade-off between the strength of coupling and operation fidelity. However, we see even small changes in the middle-donor separation, on the order of approximately 2 nm, can increase the inner-singlet contributions to the ground state from approximately 49% to approximately 98% while keeping the value of superexchange still high enough (approximately 100 MHz or approximately 1×10^{-3} meV) for use in realistic devices.

D. Electrical control of superexchange

To address the tunability of superexchange, we applied an electric field along the direction of the donor chain in our simulations, where all donors are separated by 9.7758 nm ($r_1 = r_2 = r_M = 9.7758$ nm). For a realistic applied electric field of 2 MV/m, we observe an exchange coupling of 18.09 GHz (74.83 μ eV), compared with 11.01 GHz (45.556 μ eV) under no electric field. The electric field detunes the qubits and increases the virtual tunneling between them, which results in slightly increased (less than a factor of 2) superexchange. However, when the donors are all charge neutral with one electron on each phosphorus atom, it is difficult to reach the (2,1,1,0) charge regime from a (1,1,1,1) regime without applying a very large bias. A similar challenge was observed in the work reported in Ref. [35], where on application of an electric field of 2 MV/m, the exchange coupling was increased by 5 times. In the case of superexchange, the sensitivity of the coupling with an applied electric field is even less; hence, the distanced qubits are less susceptible to charge noise caused by electric field fluctuations compared with the nearest-neighbor ones. To explore different levels of control over superexchange, we apply a J -gate bias on a system with a phosphorus-doped silicon top gate based on the original Kane architecture [14]. We place gates 30 nm above the donor plane to control the potential barrier between donor atoms and the nearest-neighbor exchange and observe their effect on superexchange. Similar three-dimensional tuning of the potential barrier between in-plane phosphorus-doped gates was recently experimentally demonstrated [49] in precision-engineered STM tunnel junctions where

the gates were degenerately phosphorus-doped silicon layers. A schematic of the system is illustrated in Fig. 5(a). The device consists of five quasimetallic gates (source, drain, and three top gates— G_1 , G_2 , and G_M). G_1 and G_2 are used to tune j_1 and j_2 , and G_M is used to tune j_M . The total electrostatic potential profile of the device in the x - z plane is shown in Fig. 5(b), where a cut is taken at the donor location. Here we see that, in the donor plane, the top gates create a parabolic potential profile. This total electrostatic potential is added to the tight-binding Hamiltonian while we are solving the energy levels of the donor quantum dots. In Figs. 5(c)–5(h), one-dimensional cuts are taken at the donor locations shown for different V_M and $V_1 (= V_2)$ values, i.e., for different voltages applied at gates G_M and G_1 (G_2), respectively. Here the source and drain are grounded, i.e., $V_S = V_D = 0$. We note that just the presence of the electrostatic leads around the donors also modifies the total electrostatic potential of the device, even without an applied voltage. This is due to the band-structure mismatch between the leads and the surrounding material, and the band-bending caused by the leads [50]. We calculate the total electrostatic potential profile of the device using a multiscale modeling technique that combines the atomistic calculation of the band structure of the gates with a nonlinear Poisson solution of the entire device [51].

1. Application of voltage to the middle top gate, G_M

Since superexchange ΔE is a function of nearest-neighbor exchanges (i.e., j_1 , j_2 , and j_M), it is necessary to understand how these exchange couplings change under an applied bias. When we apply a positive voltage to the middle gate G_M , the potential barrier between the mediators M_1 and M_2 decreases but j_M increases—see Figs. 5(c)–5(e) for increasing values of V_M . However, from the dashed line in Fig. 5(e), we see that the applied bias in G_M detunes qubits Q_1 and Q_2 with respect to M_1 and M_2 , so j_1 and j_2 will also increase. As we can see from Eq. (2), the superexchange strongly depends on the interplay between j_M and j_1 and j_2 . In our case, here the superexchange increases overall with V_M since the effect caused by detuning between the qubits and the mediator donors is stronger than that caused by lowering of the middle barrier—see the potential profile in Fig. 5(e). We observe this effect on the value of ΔE in Fig. 5(i), where we can see the superexchange as a function of V_M for $V_1 = V_2 = 0$ [case corresponding to Figs. 5(c)–5(e)]. By changing the middle-gate potential from 0 to 0.5 V, we increase the magnitude of the superexchange by a factor of 10. The increase of superexchange is due to a relatively higher increase of j_1 and j_2 than j_M , resulting in lesser singlet contribution from the mediator quantum dots, as discussed in the previous section. In our case, the singlet contribution in the middle quantum dot drops from 92.2% ($V_M = 0$) to 67% ($V_M = 0.5V$).

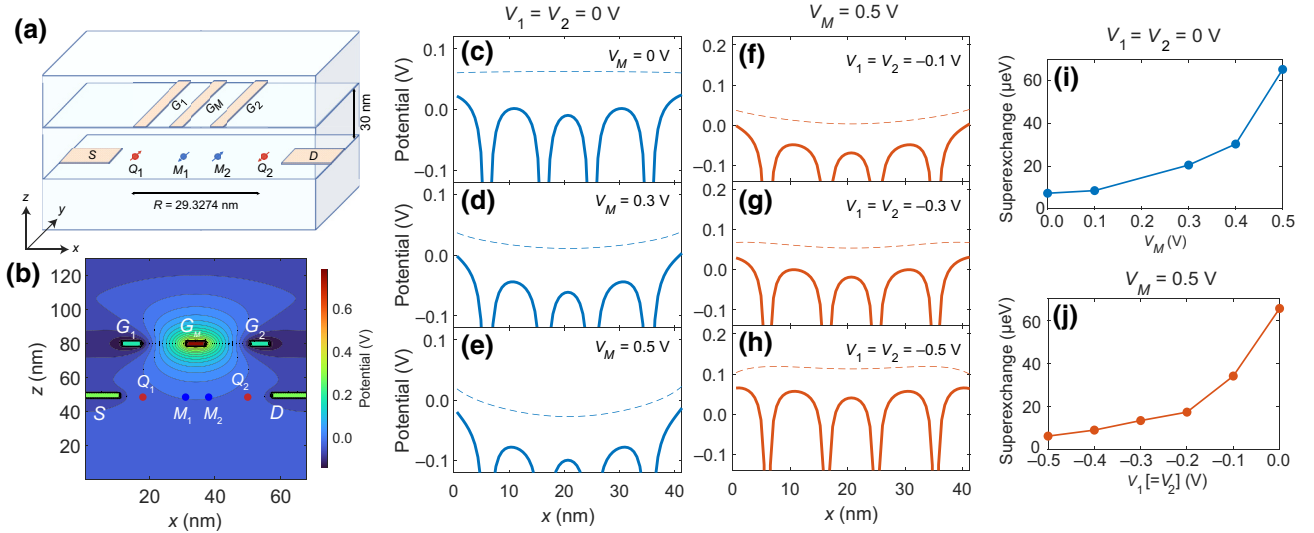


FIG. 5. Modulation of superexchange using voltage biases on phosphorus-doped top gates above the donor plane. (a) Electrostatic potential of the device in the schematic representation of the simulation domain. The qubit donor atoms (Q_1 and Q_2) and the mediator donor atoms (M_1 and M_2) are placed in the plane between the source (S) and drain (D) electrodes. Three phosphorus-doped top gates (G_1 , G_2 , and G_M) are placed 30 nm above the donor plane. (b) Total potential of the device in the x - z plane (cut taken at the donor location). Here the voltages of gates G_1 and G_2 are $V_1 = V_2 = -0.1$ V, while the middle gate G_M has voltage $V_M = 0.5$ V and the source and drain are grounded. The red and blue dots represent the location of the donors and are not to scale. (c)–(e) One-dimensional potentials with cuts taken at the donor location when $V_1 = V_2 = 0$ V and (c) $V_M = 0$ V, (d) $V_M = 0.3$ V, and (e) $V_M = 0.5$ V, respectively, as we deplete the barrier between the donors. The dashed lines represent the potential from the gates and the solid lines represent the individual donor potentials combined with the electrostatic potential from the gates. As the voltage of the top gate increases, the curvature of the potential also increases. (f)–(h) Same as (c)–(e) but when $V_M = 0.5$ V and (f) $V_1 = V_2 = -0.1$ V, (g) $V_1 = V_2 = -0.3$ V, and (h) $V_1 = V_2 = -0.5$ V, respectively. (i) Superexchange as a function of V_M when $V_1 = V_2 = 0$ V. We see that the magnitude of the superexchange increases as a positive bias is applied to G_M . The increased curvature of the applied potential of $V_M = 0.5$ V [comparison of (c),(e)] gives rise to an increase of the magnitude of superexchange by a factor of 10. (j) Superexchange as a function of $V_1 = V_2$ when $V_M = 0.5$ V. Here we see the superexchange decreases as more-negative bias is applied as a result of decreased potential curvature [comparison of (f),(h)].

2. Application of voltage to all three top gates, G_1 , G_2 , and G_M

We can minimize the detuning of qubits Q_1 and Q_2 by applying a negative voltage to the left and right gates. Then the superexchange would decrease—here from 65.42 to 6 μeV when $V_1 = V_2$ is changed from 0 to -0.5 V for $V_M = 0.5$ V; see Fig. 5(j). The positive bias applied to G_M increases j_M and the negative bias applied to $G_{1,2}$ decreases $j_{1,2}$, so the $j_{1,2}/j_M$ ratio becomes smaller. The potential profile at the donor location for $V_M = 0.5$ V and $V_1 = V_2 = -0.1$, -0.3 , and -0.5 V is shown in Figs. 5(f)–5(h). If we look at the inner-singlet contributions on the ground state, we see that the contribution has increased up to 94.05% when $V_1 = V_2 = -0.5$ V. Tuning superexchange by using three gates might be useful in increasing the fidelity of the operation; otherwise the tuning shows a similar range of superexchange even with one top gate. With these simulations, we have shown that it is possible to manipulate superexchange in a 4P chain by purely electrostatic means. Application of voltage through top gates results in better tunability of superexchange than a tilt voltage along the donor separation. We have shown that it is

possible to increase superexchange by a factor of 10 with modest gate potentials of 0.5 V. We note that even greater tunability might be desired to turn the coupling on and off for qubit operations. Such high tunability of the exchange coupling can also be achieved by depleting the middle donors. Without electrons in the middle donors, the qubits will be coupled by direct exchange, which is significantly low at these separations. On the other hand, loading electrons in the middle donors will introduce a high value of superexchange. This mechanism can be crucial for the realization of singlet-triplet oscillations in distanced qubits. We can realize the depletion of electrons from the mediator donor sites using a single-electron transistor (SET). In STM devices, a large SET is coupled to each of the donor quantum dots to perform energy-selective spin readout. The SET also functions as a reservoir for the electrons in the donor sites [12]. When selected donor levels are detuned with respect to the SET, electrons are loaded into or unloaded from selective donor dots. Similarly, with use of an SET spanning the entire donor chain, electrons can be loaded onto and depleted from the mediator quantum dots to turn the coupling on or off. Alternatively, the limited

electrical tunability of the coupling can be increased if the donors are placed further apart. The increased separation will reduce the superexchange but will increase voltage tunability because the same electric field can produce a larger detuning between the quantum dots. Schemes to account for residual direct exchange can also be adapted for superexchange to have better control over individual exchange couplings, as shown in Ref. [52]. Furthermore, different orientations, dimensions, and separations of the gates might also assist the modulation of superexchange. Although these were not achieved for the limited parameter space explored in this work, it might be possible to choose the donor separations and gate geometries optimally to increase electrical tunability of superexchange, which needs to be explored further in future work.

E. Effect of asymmetric separation of the donors

Current STM lithography techniques allow us to place donor atoms in silicon with the precision of a single lattice constant [53–57]. As a consequence, we can investigate how small shifts in the exact location of a P atom within the four-donor chain can affect the value of superexchange available. For that purpose, we analyze a chain oriented along the [100] direction with constant middle-quantum-dot separation $r_M = 5.431$ nm but with variable positions of the outer donors, described by r_1 and r_2 , where $r_1, r_2 \geq 7$ nm. We have deliberately chosen a smaller value of r_M so that $r_1, r_2 > r_M$. We do not consider nearest-neighbor separations less than 7 nm (qubit separation $R < 20$ nm) since we are interested in the long-distance qubit coupling regime and want to exceed the distance achievable by direct exchange.

The results are shown in Fig. 6. Here we can see the superexchange ΔE is maximum (11.53 GHz) for the smallest value of r_1 and r_2 ($r_1 = r_2 = 7.6$ nm). This result arises both from minimizing the total chain separation, R , and from maximizing the $r_M/r_{1,2}$ ratio—as observed in Fig. 4. ΔE decreases exponentially if either of the outer donors is moved outwards, i.e., if either r_1 or r_2 increases. However, at the same time, we can see that ΔE does not change if both of the outer donors are shifted simultaneously in the same way—see the dashed lines, where $r_1 + r_2$ is constant. This result is consistent with the Schrieffer-Wolff approximation for superexchange in Eq. (2), where the dominating contribution to ΔE comes from $j_1 j_2 / 2j_M$. While j_1 and j_2 change approximately exponentially with distance, their product will not change when $r_1 + r_2$ is kept constant.

Thus we can conclude that any small shifts in the location of the donors within the [100]-oriented chain can result in large changes in total ΔE . However, interestingly, a simultaneous shift of both outer (or both middle) donors in the same direction would not have any impact on the superexchange (indicated by the dashed black lines). The

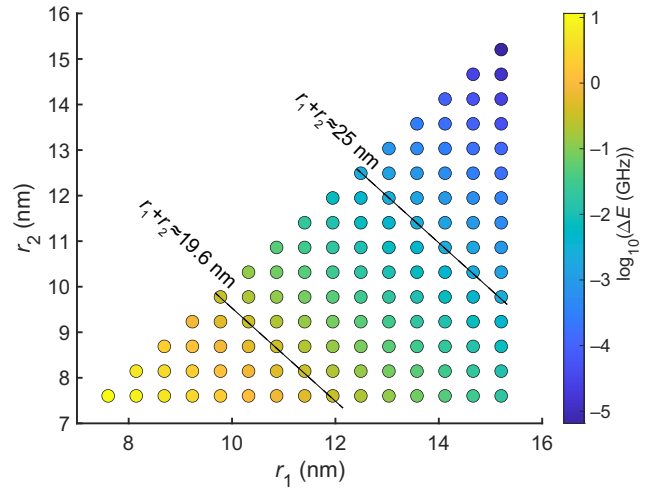


FIG. 6. Effect of donor placement on the magnitude of superexchange calculated with use of atomistic FCI along the [100] direction. Keeping the separation of the middle donors fixed ($r_M = 5.431$ nm), we change r_1 and r_2 to account for any deviation in donor placement. The superexchange ΔE is maximum when $r_1 = r_2$. We also see that ΔE remains constant when $r_1 + r_2$ is constant; see the dashed lines.

situation is completely different for the [110] crystalline direction due to the oscillations of two-donor exchange with distance, which lifts the smooth $j_1 j_2 / 2j_M$ dependency for varied r_1 and r_2 when $r_1 + r_2$ is constant. Here ΔE will change in an oscillatory manner if one middle donor or both middle donors are shifted. While we are placing the atoms, the phosphorus donors can also be shifted slightly in the [010] direction, resulting in a small angular component in the direction of separation. We investigated the impact of a small shift of the donor by one atomic lattice constant ($d_y = 0.5431$ nm) in the [010] direction. We observed that the nearest-neighbor exchange coupling reduces by a factor of 2 due to the shift, but the value is of the same order of magnitude. Hence, we expect a small change in the magnitude of superexchange due to such shifts in precision placement.

F. Impact of donor nuclear spins on the superexchange

Finally, we comment on the presence of nuclear spins in the donor system and how they can also impact superexchange and coherent electron-spin manipulation. The nuclear spins of phosphorus donor atoms couple with their electron spins through the hyperfine interaction. From the perspective of the electron spin, this can be treated as a small additional magnetic field dependent on the nuclear-spin polarization. In the case of an electron singlet-triplet spin qubit, localized within the middle double-donor quantum dot, this hyperfine interaction can create a magnetic field gradient that mixes singlet and triplet states

[17,58]. For a 1P-1P system, the gradient is approximately a few milliteslas, which gives rise to Zeeman-energy difference $\Delta E_z \approx 5 \times 10^{-4}$ meV between the donors when the two nuclear spins are oriented antiparallel ($\uparrow\downarrow$) and $\Delta E_z \approx 0$ when the two nuclear spins are aligned in the same direction ($\uparrow\uparrow$).

To create well-defined eigenstates as well as singlet and triplet states, the exchange coupling ΔE needs to dominate over ΔE_z . We can consider the four-electron system discussed in this paper essentially as two pairs of singlet-triplet qubits—one defined between the two inner quantum dots and one defined between the two outer quantum dots. To avoid mixing of the singlet and triplet states, it is desirable for both j_M and ΔE to be significantly greater than ΔE_z . From Fig. 2, this is satisfied when the middle-donor separation r_M is smaller than 10–15 nm, which includes most of the results presented in this work. The superexchange ΔE ultimately depends both on r_M and R . From Fig. 4 we can see it is possible to design 4P configurations that belong to the regime where $j_1, j_2/j_M < 0.3$ and at the same time satisfy $\Delta E > \Delta E_z$. These considerations are, however, no longer relevant if we deterministically initialize the nuclear spins to be all parallel before any operation using a local nuclear magnetic resonance [10]. In this case, there is no magnetic field gradient and thus no limitations on the minimum values of j_M and ΔE .

IV. CONCLUSION

In this work, we have presented the results for strong non-nearest-neighbor exchange coupling over a long distance (20–35 nm) with a possible extension of up to 45 nm, which has not been explored in donor quantum dots before. Using an atomistic full-configuration-interaction technique, we have calculated the eigenvalues of a four-electron system with high-quality atomistic basis states and have provided a comparison with an effective spin Hamiltonian to determine the viability of our intensive numerical calculations. We have shown that by our placing the mediator donors one atomic position inwards compared with the symmetric chain, it is possible to enable coherent control of the qubits separated in the [100] and [110] directions. Similarly to previous work on direct exchange, we observe a monotonic dependence of superexchange versus distance for donors separated in the [100] direction and an oscillatory dependence for donors separated in the [110] direction. Importantly, we have demonstrated that the superexchange can be increased by an order of magnitude by purely electrostatic means using realistic experimental gate voltages. These results pave the way for the realization of fast singlet-triplet control for distanced qubits. The calculations support the experimental realization of long-distance coupling of donor qubits in silicon.

- [1] J. T. Muhonen, J. P. Dehollain, A. Laucht, F. E. Hudson, R. Kalra, T. Sekiguchi, K. M. Itoh, D. N. Jamieson, J. C. McCallum, A. S. Dzurak, and A. Morello, Storing quantum information for 30 seconds in a nanoelectronic device, *Nat. Nanotechnol.* **9**, 986 (2014).
- [2] M. Steger, K. Saeedi, M. L. W. Thewalt, J. J. L. Morton, H. Riemann, N. V. Abrosimov, P. Becker, and H.-J. Pohl, Quantum information storage for over 180 s using donor spins in a ^{28}Si “semiconductor vacuum”, *Science* **336**, 1280 (2012).
- [3] A. M. Tyryshkin, S. Tojo, J. J. L. Morton, H. Riemann, N. V. Abrosimov, P. Becker, H.-J. Pohl, T. Schenkel, M. L. W. Thewalt, K. M. Itoh, and S. A. Lyon, Electron spin coherence exceeding seconds in high-purity silicon, *Nat. Mater.* **11**, 143 (2012).
- [4] S. R. Schofield, N. J. Curson, M. Y. Simmons, F. J. Rueß, T. Hallam, L. Oberbeck, and R. G. Clark, Atomically precise placement of single dopants in Si, *Phys. Rev. Lett.* **91**, 136104 (2003).
- [5] R. G. Clark *et al.* Progress in silicon-based quantum computing, *Philos. Trans. R. Soc. London, A* **361**, 1451 (2003).
- [6] M. Simmons, F. Ruess, K. Goh, T. Hallam, S. Schofield, L. Oberbeck, N. Curson, A. Hamilton, M. Butcher, R. Clark, and T. Reusch, Scanning probe microscopy for silicon device fabrication, *Mol. Simul.* **31**, 505 (2005).
- [7] F. J. Rueß, W. Pok, T. C. G. Reusch, M. J. Butcher, K. E. J. Goh, L. Oberbeck, G. Scappucci, A. R. Hamilton, and M. Y. Simmons, Realization of atomically controlled dopant devices in silicon, *Small* **3**, 563 (2007).
- [8] M. Fuechle, J. A. Miwa, S. Mahapatra, H. Ryu, S. Lee, O. Warschkow, L. C. L. Hollenberg, G. Klimeck, and M. Y. Simmons, A single-atom transistor, *Nat. Nanotechnol.* **7**, 242 (2012).
- [9] A. Morello, J. J. Pla, F. A. Zwanenburg, K. W. Chan, K. Y. Tan, H. Huebl, M. Möttönen, C. D. Nugroho, C. Yang, J. A. van Donkelaar, A. D. C. Alves, D. N. Jamieson, C. C. Escott, L. C. L. Hollenberg, R. G. Clark, and A. S. Dzurak, Single-shot readout of an electron spin in silicon, *Nature* **467**, 687 (2010).
- [10] J. J. Pla, K. Y. Tan, J. P. Dehollain, W. H. Lim, J. J. L. Morton, D. N. Jamieson, A. S. Dzurak, and A. Morello, A single-atom electron spin qubit in silicon, *Nature* **489**, 541 (2012).
- [11] J. J. Pla, K. Y. Tan, J. P. Dehollain, W. H. Lim, J. J. L. Morton, F. A. Zwanenburg, D. N. Jamieson, A. S. Dzurak, and A. Morello, High-fidelity readout and control of a nuclear spin qubit in silicon, *Nature* **496**, 334 (2013).
- [12] Y. He, S. K. Gorman, D. Keith, L. Kranz, J. G. Keizer, and M. Y. Simmons, A two-qubit gate between phosphorus donor electrons in silicon, *Nature* **571**, 371 (2019).
- [13] M. T. Maźdik, *et al.*, Precision tomography of a three-qubit donor quantum processor in silicon, *Nature* **601**, 348 (2022).
- [14] B. E. Kane, A silicon-based nuclear spin quantum computer, *Nature* **393**, 133 (1998).
- [15] G. Tosi, F. A. Mohiyaddin, V. Schmitt, S. Tenberg, R. Rahman, G. Klimeck, and A. Morello, Silicon quantum processor with robust long-distance qubit couplings, *Nat. Commun.* **8**, 450 (2017).
- [16] K. J. Morse, R. J. S. Abraham, A. DeAbreu, C. Bowness, T. S. Richards, H. Riemann, N. V. Abrosimov, P. Becker, H.-J.

- Pohl, M. L. W. Thewalt, and S. Simmons, A photonic platform for donor spin qubits in silicon, *Sci. Adv.* **3**, e1700930 (2017).
- [17] E. N. Osika, S. K. Gorman, S. Monir, Y.-L. Hsueh, M. Borszcz, H. Geng, B. Thorgrimsson, M. Y. Simmons, and R. Rahman, Shelving and latching spin readout in atom qubits in silicon, *Phys. Rev. B* **106**, 075418 (2022).
- [18] L. M. K. Vandersypen, H. Bluhm, J. S. Clarke, A. S. Dzurak, R. Ishihara, A. Morello, D. J. Reilly, L. R. Schreiber, and M. Veldhorst, Interfacing spin qubits in quantum dots and donors—hot, dense, and coherent, *npj Quantum Inf.* **3**, 1 (2017).
- [19] M. Kiczynski, S. K. Gorman, H. Geng, M. B. Donnelly, Y. Chung, Y. He, J. G. Keizer, and M. Y. Simmons, Engineering topological states in atom-based semiconductor quantum dots, *Nature* **606**, 694 (2022).
- [20] K. W. Chan, H. Sahasrabudhe, W. Huang, Y. Wang, H. C. Yang, M. Veldhorst, J. C. C. Hwang, F. A. Mohiyaddin, F. E. Hudson, K. M. Itoh, A. Saraiva, A. Morello, A. Laucht, R. Rahman, and A. S. Dzurak, Exchange coupling in a linear chain of three quantum-dot spin qubits in silicon, *Nano Lett.* **21**, 1517 (2021).
- [21] K. Deng and E. Barnes, Interplay of exchange and superexchange in triple quantum dots, *Phys. Rev. B* **102**, 035427 (2020).
- [22] M. J. Rančić and G. Burkard, Ultracoherent operation of spin qubits with superexchange coupling, *Phys. Rev. B* **96**, 201304 (2017).
- [23] T. A. Baart, T. Fujita, C. Reichl, W. Wegscheider, and L. M. K. Vandersypen, Coherent spin-exchange via a quantum mediator, *Nat. Nanotechnol.* **12**, 26 (2017).
- [24] S. Mehl, H. Bluhm, and D. P. DiVincenzo, Two-qubit couplings of singlet-triplet qubits mediated by one quantum state, *Phys. Rev. B* **90**, 045404 (2014).
- [25] F. K. Malinowski, F. Martins, T. B. Smith, S. D. Bartlett, A. C. Doherty, P. D. Nissen, S. Fallahi, G. C. Gardner, M. J. Manfra, C. M. Marcus, and F. Kuemmeth, Fast spin exchange across a multielectron mediator, *Nat. Commun.* **10**, 1196 (2019).
- [26] F. K. Malinowski, F. Martins, T. B. Smith, S. D. Bartlett, A. C. Doherty, P. D. Nissen, S. Fallahi, G. C. Gardner, M. J. Manfra, C. M. Marcus, and F. Kuemmeth, Spin of a multi-electron quantum dot and its interaction with a neighboring electron, *Phys. Rev. X* **8**, 011045 (2018).
- [27] K. Deng, F. A. Calderon-Vargas, N. J. Mayhall, and E. Barnes, Negative exchange interactions in coupled few-electron quantum dots, *Phys. Rev. B* **97**, 245301 (2018).
- [28] X. Croot, S. Pauka, J. Watson, G. Gardner, S. Fallahi, M. Manfra, and D. Reilly, Device architecture for coupling spin qubits via an intermediate quantum state, *Phys. Rev. Appl.* **10**, 044058 (2018).
- [29] V. Srinivasa, H. Xu, and J. Taylor, Tunable spin-qubit coupling mediated by a multielectron quantum dot, *Phys. Rev. Lett.* **114**, 226803 (2015).
- [30] H. Qiao, Y. P. Kandel, S. Fallahi, G. C. Gardner, M. J. Manfra, X. Hu, and J. M. Nichol, Long-distance superexchange between semiconductor quantum-dot electron spins, *Phys. Rev. Lett.* **126**, 017701 (2021).
- [31] J. Fei, D. Zhou, Y.-P. Shim, S. Oh, X. Hu, and M. Friesen, Mediated gates between spin qubits, *Phys. Rev. A* **86**, 062328 (2012).
- [32] A. K. Ramdas and S. Rodriguez, Spectroscopy of the solid-state analogues of the hydrogen atom: Donors and acceptors in semiconductors, *Rep. Progr. Phys.* **44**, 1297 (1981).
- [33] A. Tankasala, B. Voisin, Z. Kembrely, J. Salfi, Y.-L. Hsueh, E. N. Osika, S. Rogge, and R. Rahman, Shallow dopant pairs in silicon: An atomistic full configuration interaction study, *Phys. Rev. B* **105**, 155158 (2022).
- [34] B. Voisin, J. Bocquel, A. Tankasala, M. Usman, J. Salfi, R. Rahman, M. Y. Simmons, L. C. L. Hollenberg, and S. Rogge, Valley interference and spin exchange at the atomic scale in silicon, *Nat. Commun.* **11**, 1 (2020).
- [35] Y. Wang, A. Tankasala, L. C. L. Hollenberg, G. Klimeck, M. Y. Simmons, and R. Rahman, Highly tunable exchange in donor qubits in silicon, *npj Quantum Inf.* **2**, 1 (2016).
- [36] A. Szabo and N. S. Ostlund, *Modern Quantum Chemistry: Introduction to Advanced Electronic Structure Theory* (Dover Publications, New York, 1996).
- [37] G. X. Chan and X. Wang, Sign switching of superexchange mediated by a few electrons in a nonuniform magnetic field, *Phys. Rev. A* **106**, 022420 (2022).
- [38] A. L. Saraiva, A. Baena, M. J. Calderón, and B. Koiller, Theory of one and two donors in silicon, *J. Phys.: Condens. Matter* **27**, 154208 (2015).
- [39] B. Joecker, A. D. Baczewski, J. K. Gamble, J. J. Pla, A. Saraiva, and A. Morello, Full configuration interaction simulations of exchange-coupled donors in silicon using multi-valley effective mass theory, *New J. Phys.* **23**, 073007 (2021).
- [40] A. Tankasala, J. Salfi, J. Bocquel, B. Voisin, M. Usman, G. Klimeck, M. Y. Simmons, L. C. L. Hollenberg, S. Rogge, and R. Rahman, Two-electron states of a group-V donor in silicon from atomistic full configuration interactions, *Phys. Rev. B* **97**, 195301 (2018).
- [41] S. Ahmed, N. Kharche, R. Rahman, M. Usman, S. Lee, H. Ryu, H. Bae, S. Clark, B. Haley, M. Naumov, F. Saied, M. Korkusinski, R. Kennel, M. McLennan, T. B. Boykin, and G. Klimeck, Multimillion atom simulations with NEMO 3-D, *ArXiv:0901.1890* (2009).
- [42] G. Klimeck, S. Ahmed, H. Bae, N. Kharche, S. Clark, B. Haley, S. Lee, M. Naumov, H. Ryu, F. Saied, M. Prada, M. Korkusinski, T. Boykin, and R. Rahman, Atomistic simulation of realistically sized nanodevices using NEMO 3-D—part I: Models and benchmarks, *IEEE Trans. Electron. Devices* **54**, 2079 (2007).
- [43] T. B. Boykin, G. Klimeck, and F. Oyafuso, Valence band effective-mass expressions in the $sp^3d^5s^*$ empirical tight-binding model applied to a Si and Ge parametrization, *Phys. Rev. B* **69**, 115201 (2004).
- [44] R. Rahman, C. J. Wellard, F. R. Bradbury, M. Prada, J. H. Cole, G. Klimeck, and L. C. L. Hollenberg, High precision quantum control of single donor spins in silicon, *Phys. Rev. Lett.* **99**, 036403 (2007).
- [45] R. Rahman, G. P. Lansbergen, S. H. Park, J. Verduijn, G. Klimeck, S. Rogge, and L. C. L. Hollenberg, Orbital Stark effect and quantum confinement transition of donors in silicon, *Phys. Rev. B* **80**, 165314 (2009).
- [46] See Supplemental Material at <http://link.aps.org/supplemental/10.1103/PhysRevApplied.21.014038> for the convergence of superexchange for four different configurations, analysis of single-electron wave functions in terms

- of the Slater determinants, and contributions of inner-singlet states to the ground state of the four-electron problem.
- [47] C. G. Baker, U. L. Hetmaniuk, R. B. Lehoucq, and H. K. Thornquist, Anasazi software for the numerical solution of large-scale eigenvalue problems, *ACM Trans. Math. Softw.* **36**, 1 (2009).
- [48] B. Koiller, X. Hu, and S. D. Sarma, Exchange in silicon-based quantum computer architecture, *Phys. Rev. Lett.* **88**, 027903 (2001).
- [49] M. B. Donnelly, J. G. Keizer, Y. Chung, and M. Y. Simmons, Monolithic three-dimensional tuning of an atomically defined silicon tunnel junction, *Nano Lett.* **21**, 10092 (2021).
- [50] H. Ryu, S. Lee, B. Weber, S. Mahapatra, L. C. Hollenberg, M. Y. Simmons, and G. Klimeck, Atomistic modeling of metallic nanowires in silicon, *Nanoscale* **5**, 8666 (2013).
- [51] M. B. Donnelly, M. M. Munia, J. G. Keizer, Y. Chung, A. S.-E. Huq, E. N. Osika, Y.-L. Hsueh, R. Rahman, and M. Y. Simmons, Multi-scale modeling of tunneling in nanoscale atomically precise Si:P tunnel junctions, *Adv. Funct. Mater.* **33**, 2214011 (2023).
- [52] I. Heinz, A. R. Mills, J. R. Petta, and G. Burkard, Analysis and mitigation of residual exchange coupling in linear spin qubit arrays, Preprint [ArXiv:2308.11308](https://arxiv.org/abs/2308.11308) (2023).
- [53] M. Fuechsle, J. A. Miwa, S. Mahapatra, H. Ryu, S. Lee, O. Warschkow, L. C. Hollenberg, G. Klimeck, and M. Y. Simmons, A single-atom transistor, *Nat. Nanotechnol.* **7**, 242 (2012).
- [54] J. A. Ivie, Q. Campbell, J. C. Koepke, M. I. Brickson, P. A. Schultz, R. P. Muller, A. M. Mounce, D. R. Ward, M. S. Carroll, E. Bussmann, A. D. Baczewski, and S. Misra, Impact of incorporation kinetics on device fabrication with atomic precision, *Phys. Rev. Appl.* **16**, 054037 (2021).
- [55] E. Bussmann, R. E. Butera, J. H. Owen, J. N. Randall, S. M. Rinaldi, A. D. Baczewski, and S. Misra, Atomic-precision advanced manufacturing for Si quantum computing, *MRS Bull.* **46**, 607 (2021).
- [56] M. Y. Simmons and J. Keizer, Method for selective incorporation of dopant atoms in a semiconductive surface. U.S. Patent, US11227768 B2 (2022).
- [57] J. Wyrick, X. Wang, P. Namboodiri, R. V. Kashid, F. Fei, J. Fox, and R. Silver, Enhanced atomic precision fabrication by adsorption of phosphine into engineered dangling bonds on H-Si using STM and DFT, *ACS Nano* **16**, 19114 (2022).
- [58] L. Kranz, S. K. Gorman, B. Thorgrimsson, S. Monir, Y. He, D. Keith, K. Charde, J. G. Keizer, R. Rahman, and M. Y. Simmons, The use of exchange coupled atom qubits as atomic-scale magnetic field sensors, *Adv. Mater.* **35**, 2201625 (2023).